Supporting information for

Porous Pb-Doped ZnO Nanobelts with Enriched Oxygen Vacancies: Preparation and Their Chemiresistive Sensing Performance

Kai-Ge Zheng [1,2], Tian-Yu Yang [1,2] and Zheng Guo [1,2,*]

[1] Information Materials and Intelligent Sensing Laboratory of Anhui Province, Institutes of Physical Science and Information Technology, Anhui University, Hefei 230601, China

[2] Key Laboratory of Structure and Functional Regulation of Hybrid Materials (Anhui University), Ministry of Education, Hefei 230601, China

*Correspondence should be addressed to Z. Guo.

E-mail: zhguo@ahu.edu.cn (Z. Guo)

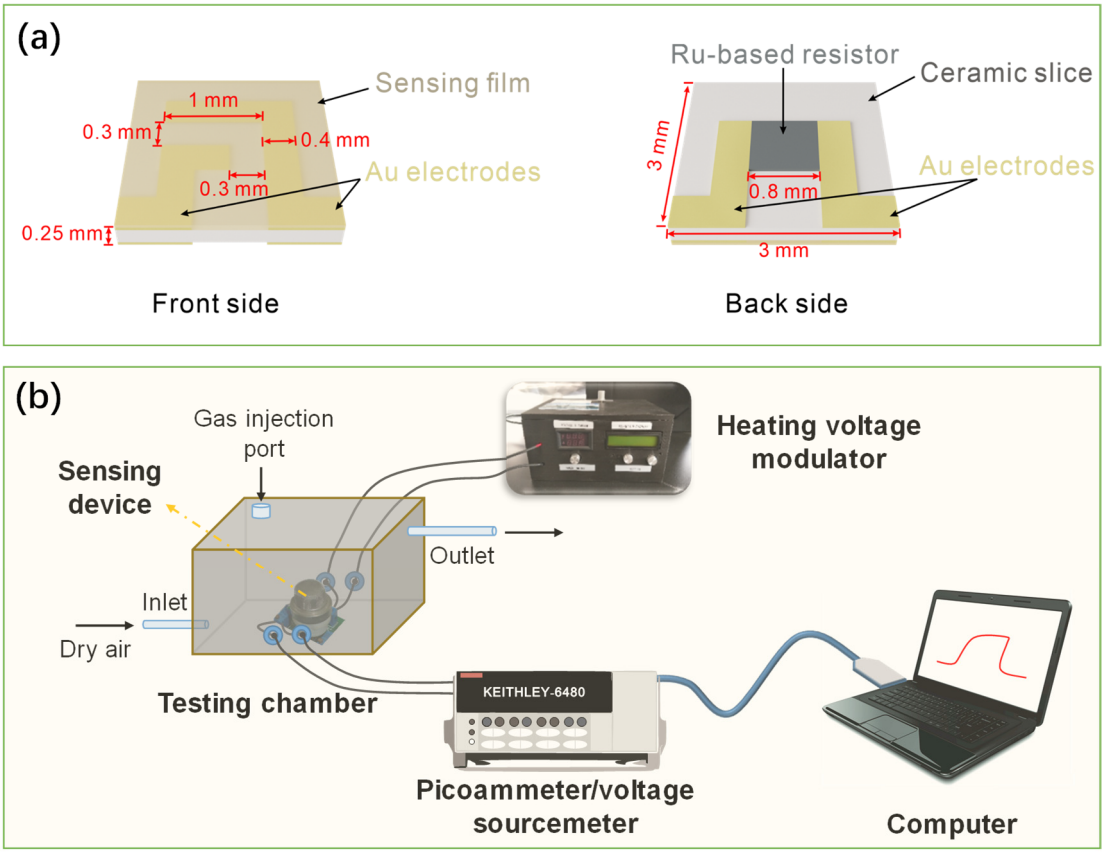

Figure S1. (a) Structure of the as-fabricated sensing device, (b) Schematic setup of gas-sensing measurement.

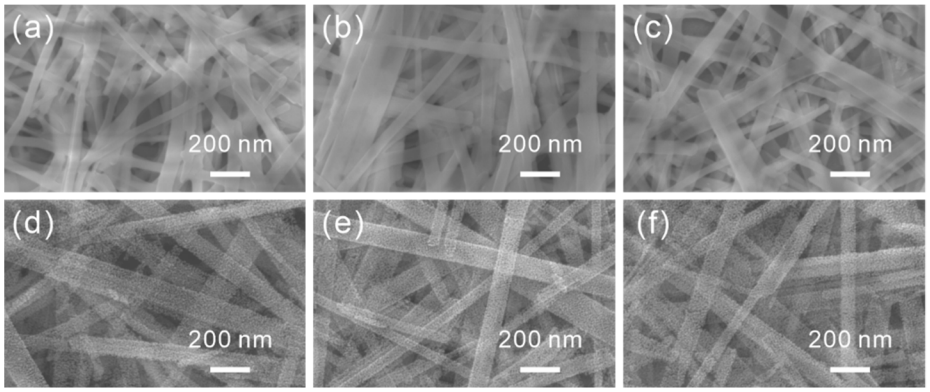

Figure S2. SEM images of 0.44 at% (a), 1.39 at% (b) and 2.01 at% (c) Pb^{2+}-exchanged ZnSe precursor nanobelts, and 0.44 at% (d), 1.39 at% (e) and 2.01 at% (f) Pb-doped ZnO porous nanobelts.

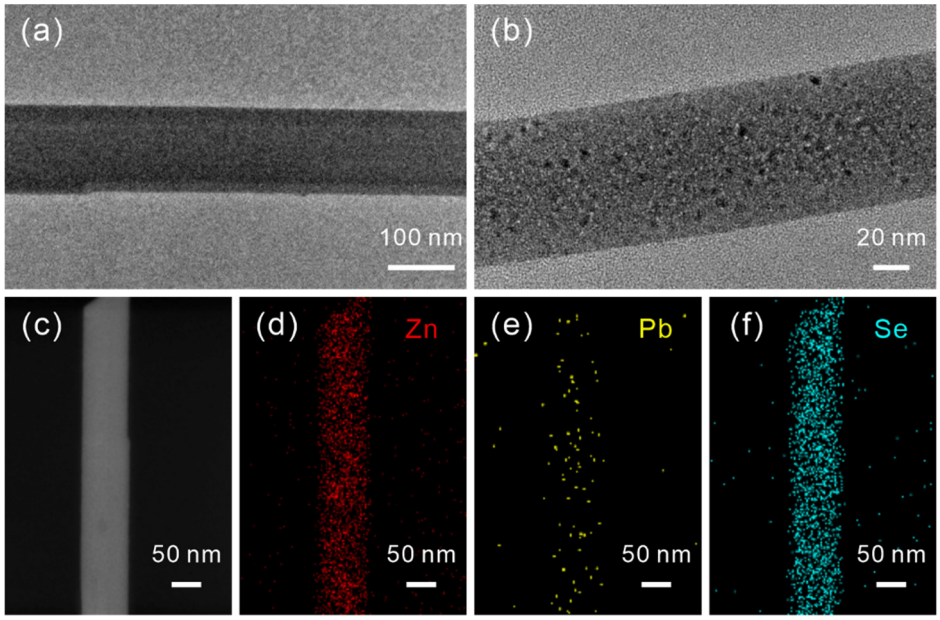

Figure S3. (a) TEM image of single Pb-doped precursor nanobelt, (b) its high magnified TEM, (c) its HAADF image and the corresponding elemental mapping patterns of (d) Zn, (e) Pb and (f) Se.

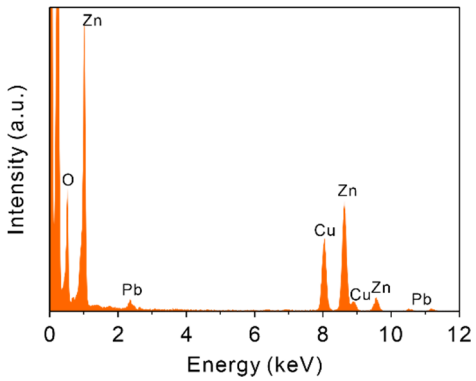

Figure S4. EDX spectrum of the obtained Pb-doped ZnO porous nanobelts.

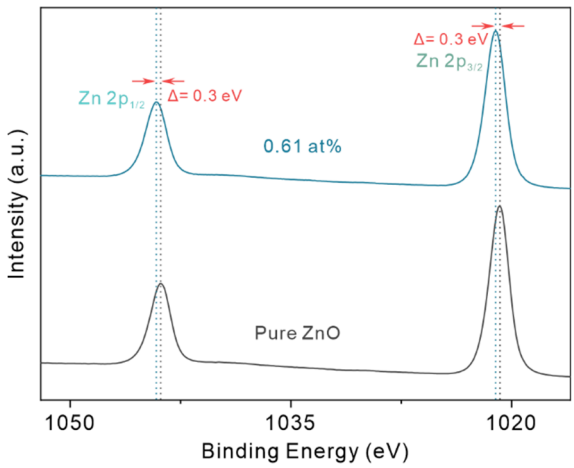

Figure S5. High-resolution Zn 2p XPS spectra of pure ZnO porous nanobelts and 0.61 at% Pb-doped ZnO porous nanobelts.

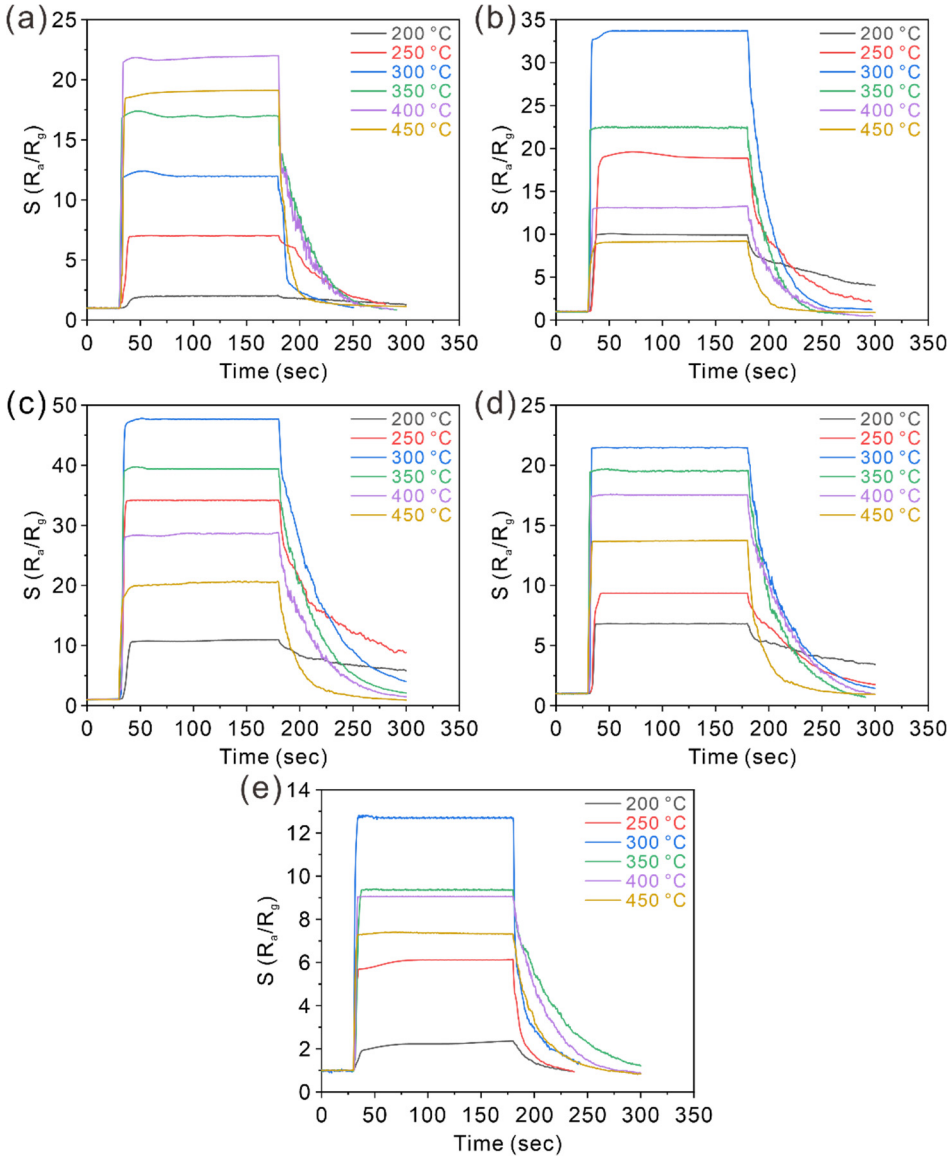

Figure S6. The real-time response curves of porous ZnO nanobelts doped with (a) 0 at%, (b) 0.44 at%, (c) 0.61 at%, (d) 1.39 at% and (e) 2.01 at% of Pb toward 50 ppm of n-butanol at different working temperature.

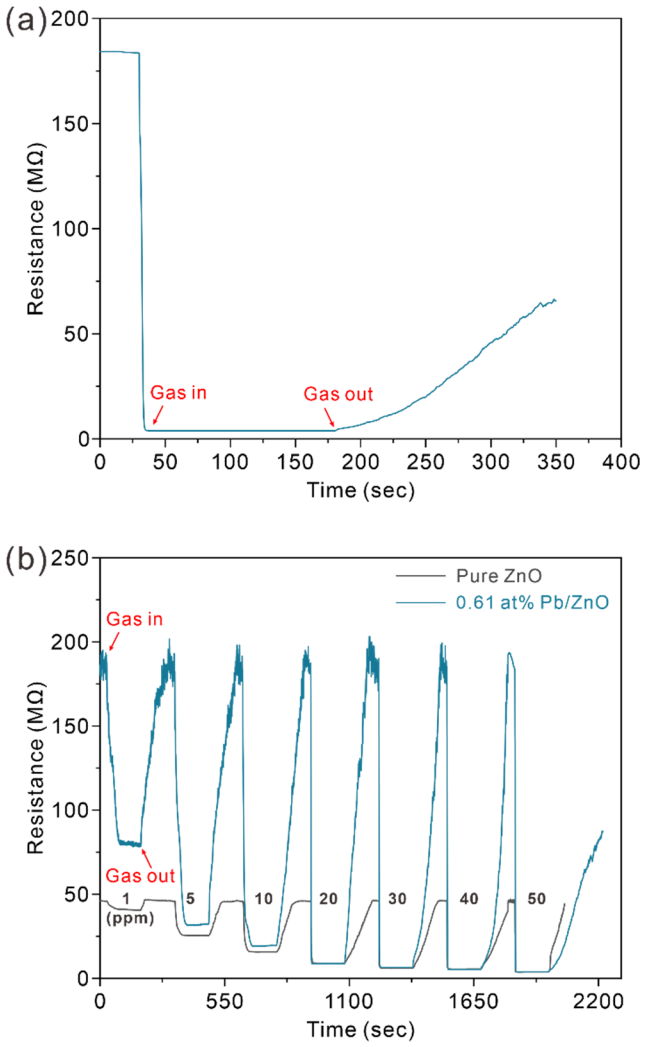

Figure S7. (a) The real-time resistance response curve of 0.61 at% Pb-doped ZnO porous nanobelts toward 50 ppm of n-butanol at 300 °C, (b)The real-time resistance curve of pure ZnO porous nanobelts and 0.61 at% Pb-doped ZnO porous nanobelts toward different concentrations of n-butanol at 300 °C.

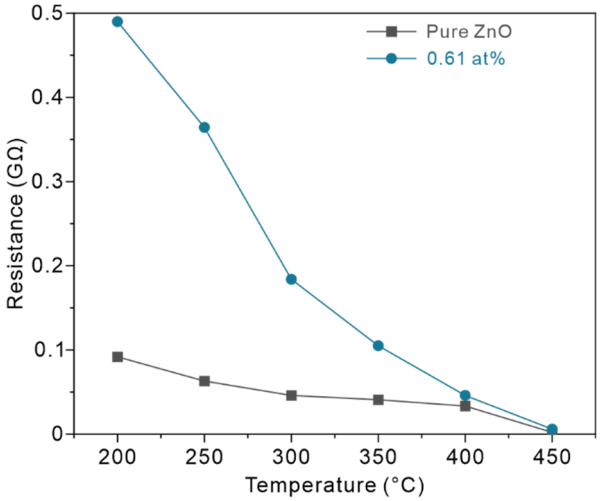

Figure S8. The relationship between resistance and temperature of the sensing film fabricated with pure ZnO porous nanobelts and 0.61 at% Pb-doped ZnO porous nanobelts.

Table S1. Structural parameters of as-synthesized samples analyzed at (100) from XRD data.

Pb (at%)	2θ (deg.)	d (Å)	Lattice parameters		FWHM (deg.)
			a (Å)	c (Å)	
0	31.858	2.8067	3.24583	5.20234	0.719
0.44	31.837	2.8085	3.24644	5.20374	0.61
0.61	31.829	2.8091	3.24774	5.20593	0.68
1.39	31.816	2.8103	3.24811	5.20637	0.625
2.0	31.766	2.8146	3.25184	5.21353	0.716

Table S2. Fitting results of O 1s XPS spectrum of pure ZnO porous nanobelts and 0.61 at% Pb-doped ZnO porous nanobelts.

Samples	Oxygen species	Binding energy (eV)	Relative percentage (%)
ZnO	O_{ad}	531.84	12.47
	O_{va}	531.06	13.62
	O_{Zn}	530.27	73.91
Pb-doped ZnO (0.61 at%)	O_{ad}	531.68	20.63
	O_{va}	530.66	30.13
	O_{Zn}	530.2	48.75
	O_{Pb}	530.37	0.49

Table S3. Relative response of various metal oxide nanostructures toward n-butanol, A reported in the literatures and the present work.

Sensing materials	Concentration (ppm)	Response	Temperature (°C)	Response time (s)	Reference
SnO_2 hollow cubes	50	40	310	2.1	[1]
In_2O_3/ZnO nanorods	50	50	370	6	[2]
ZnO nanorod-microflower	50	38.2	300	8	[3]
(CuO-Cu_2O)/ZnO	100	3	350	8.2	[4]
In_2O_3 nanorods	50	200	240	77.5	[5]
ZrO_2/ZnO nanorods	50	30	245	20	[6]
$ZnFe_2O_4$/ZnO microspheres	50	13	320	10	[7]
Porous Co_3O_4	100	21	100	146	[8]
$Au_{39}Rh_{61}$-urchinlike $W_{18}O_{49}$	50	10	260	2	[9]
ZnO@TiO_2 nanorods	100	6.7	200	17	[10]
Sb-doped $ZnFe_2O_4$ MPs	100	35.5	250	4	[11]
Au-WO_3	100	14.4	250	10	[12]
In_2O_3@ZnS hollow spheres	100	8.6	260	20	[13]
$NiCo_2O_4$	100	3.4	165	68	[14]
Pb-doped ZnO porous nanobelts	**50**	**47.7**	**300**	**5**	**This work**

Reference:

[1] Y. Wang, Y. Zeng, L. Wang, Z. Lou, L. Qiao, H. Tian, et al., Ultrathin nanorod-assembled SnO_2 hollow cubes for high sensitive n-butanol detection, Sensors and Actuators B: Chemical, 283(2019) 693-704.

[2] F. Liu, G. Huang, X. Wang, X. Xie, G. Xu, G. Lu, et al., High response and selectivity of single crystalline ZnO nanorods modified by In_2O_3 nanoparticles for n-butanol gas sensing, Sensors and Actuators B: Chemical, 277(2018) 144-51.

[3] W. Yang, X. Xiao, B. Fang, H. Deng, Nanorods-assembled ZnO microflower as a powerful channel for n-butanol sensing, Journal of Alloys and Compounds, 860(2021) 158410.

[4] M. Hoppe, N. Ababii, V. Postica, O. Lupan, O. Polonskyi, F. Schütt, et al., (CuO-Cu_2O)/ZnO:Al heterojunctions for volatile organic compound detection, Sensors and Actuators B: Chemical, 255(2018) 1362-75.

[5] R. Zhao, Q. Wei, Y. Ran, Y. Kong, D. Ma, L. Su, et al., One-dimensional In_2O_3 nanorods as sensing material for ppb-level n-butanol detection, Nanotechnology, 32(2021) 375501.

[6] W. Li, Y. Ren, Y. Guo, ZrO2/ZnO nanocomposite materials for chemiresistive butanol sensors, Sensors and Actuators B: Chemical, 308(2020) 127658.

[7] S. Wang, X. Gao, J. Yang, Z. Zhu, H. Zhang, Y. Wang, Synthesis and gas sensor application of $ZnFe_2O_4$–ZnO composite hollow microspheres, RSC Adv, 4(2014) 57967-74.
[8] M. Wang, Z. Shen, X. Zhao, F. Duanmu, H. Yu, H. Ji, Rational shape control of porous Co_3O_4 assemblies derived from MOF and their structural effects on n-butanol sensing, J Hazard Mater, 371(2019) 352-61.
[9] J. Bai, Y. Li, Y. Liu, H. Wang, F. Liu, F. Liu, et al., Au39Rh61 Alloy Nanocrystal-Decorated $W_{18}O_{49}$ for Enhanced Detection of n-Butanol, ACS Sens, 4(2019) 2662-70.
[10] Y. Xu, L. Zheng, C. Yang, W. Zheng, X. Liu, J. Zhang, Chemiresistive sensors based on core-shell ZnO@TiO_2 nanorods designed by atomic layer deposition for n-butanol detection, Sensors and Actuators B: Chemical, 310(2020) 127846.
[11] L. Lv, P. Cheng, Y. Wang, L. Xu, B. Zhang, C. Lv, et al., Sb-doped three-dimensional $ZnFe_2O_4$ macroporous spheres for N-butanol chemiresistive gas sensors, Sensors and Actuators B: Chemical, 320(2020) 128384.
[12] Y. Wang, B. Zhang, J. Liu, Q. Yang, X. Cui, Y. Gao, et al., Au-loaded mesoporous WO_3: Preparation and n-butanol sensing performances, Sensors and Actuators B: Chemical, 236(2016) 67-76.
[13] P. He, H. Fu, X. Yang, S. Xiong, D. Han, X. An, Variable gas sensing performance towards different volatile organic compounds caused by integration types of ZnS on In_2O_3 hollow spheres, Sensors and Actuators B: Chemical, 345(2021) 130316.
[14] F. Dang, Y. Wang, J. Gao, L. Xu, P. Cheng, L. Lv, et al., Hierarchical flower-like $NiCo_2O_4$ applied in n-butanol detection at low temperature, Sensors and Actuators B: Chemical, 320(2020) 128577.